INTERNATIONAL JOURNAL FOR NUMERICAL METHODS IN FLUIDS, VOL. 1, 145–169 (1981)

# EFFECT OF OPEN BOUNDARY CONDITION ON NUMERICAL SIMULATION OF THREE-DIMENSIONAL HYDROTHERMAL BEHAVIOR OF BISCAYNE BAY, FLORIDA

SUBRATA SENGUPTA

*University of Miami, Coral Gables, Florida 33124, U.S.A.*

H. P. MILLER

*United Engineers and Constructors Inc., Philadelphia, Pennsylvania, U.S.A.*

AND

SAMUEL S. LEE

*University of Miami, Coral Gables, Florida 33124, U.S.A.*

## SUMMARY

A three-dimensional time dependent free-surface model has been used to simulate the velocity and temperature distributions in Biscayne Bay, an estuarine basin in South Florida. Comparisons with tide gauge data and airborne infrared temperature data have been made. Analyses of three-dimensional velocity structure, phase relationships of velocity with depth and horizontal location have been conducted.

One of the major concerns with three-dimensional models is the specification of conditions at open-boundaries, since it is rare that complete time dependent variations of variables at these boundaries are available. Two sets of approximate boundary conditions at the Biscayne Bay–Atlantic Ocean interface have been used for computations. It was found that specification of averaged surface height variation at open boundaries yield significantly better results than specification of estimated values of velocity.

KEY WORDS Numerical Model Estuary Open Boundary Condition Three dimensional Hydrothermal Biscayne Bay

## INTRODUCTION

With the growing interest in prediction of man's impact on aquatic ecosystems, recent studies have been conducted in numerical modelling of associated hydrodynamic and thermodynamic processes occurring in various types of water bodies.[1] The three-dimensional, time-dependent conservation equations presented in this paper yield numerical solutions for the circulation, tide-level variations, and temperature distribution occurring on a particular day in the South Biscayne Bay in Florida. Investigators such as Leendertse[2] have also modelled tide dominated estuarine circulation. Blumberg[3,4] applied his numerical tidal model to Chesapeake Bay, and Reid and Bodine[5] investigated numerically, with a similar model, the Galveston Bay. Fischer[6] provides an excellent review of mixing and dispersion in estuaries.

Two significant modelling efforts exist for the South Biscayne Bay shown in Figure 1.

0271–2091/81/020145–25$02.50 *Received October 1980*

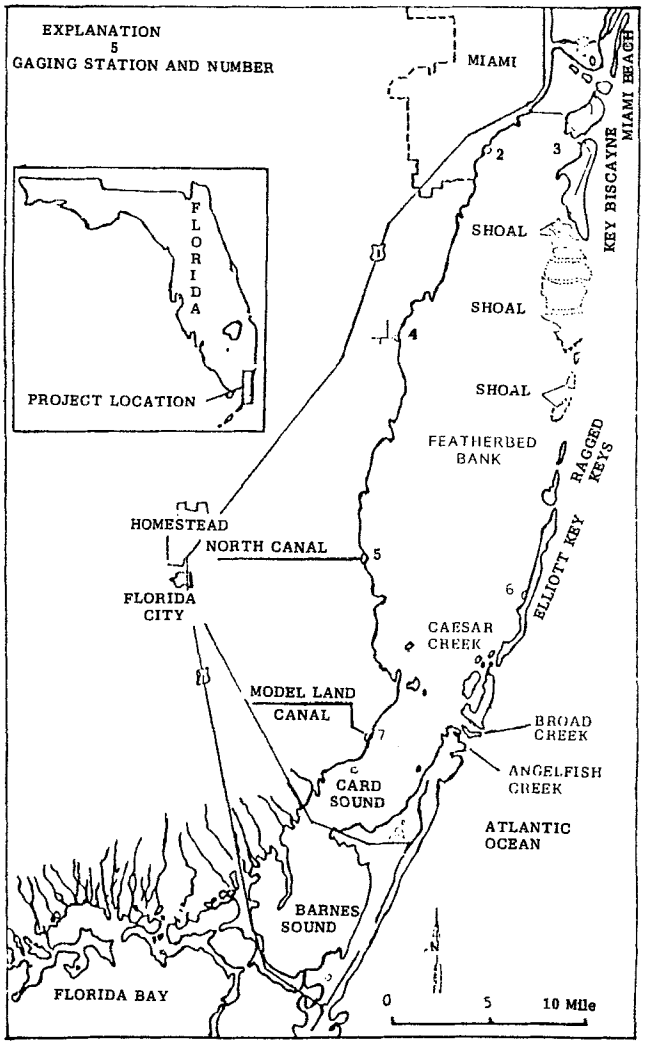


Figure 1. Map of Biscayne Bay

Verma and Dean[7] used vertically integrated momentum equations to predict surface elevations and mass transport for the South Biscayne Bay–Card Sound basin. They incorporated tidal effects and approximated the effects of shallow sills at the ocean–bay interface by using friction factors at the basin's bottom. A three-dimensional rigid-lid formulation for the bay was investigated by Sengupta *et al.*[8,9] However, the major drawback of the formulation was the rigid-lid approximation, whereby surface elevation effects and tidal driving mechanisms, at the ocean–bay interface, could not be modelled adequately. Therefore, the free surface model provides a more realistic approach to the numerical investigation of the bay's hydromechanics and associated tidal dynamics.

A numerical free surface model has been calibrated and verified by utilizing both *in situ* measurements of currents and temperature, and, also, by employing airborne infrared thermal scanner data. The proper behavior of the numerical solutions was further verified by comparison of model predicted water tide levels with an existing tide data base for the bay as compiled by Schneider.[10] The effects of salinity have been ignored as a first approximation. Blumberg[11] has demonstrated that for simulation of gross features such as total discharge, range and tidal phase, salinity is not important.

Sengupta *et al.*[12] have presented elsewhere some results of this numerical modelling effort for South Biscayne Bay. However, the aim of this paper is to further illustrate the salient features of these numerical results, and the effect of ocean–bay boundary conditions. Thus, this presentation will be more comprehensive in its nature, especially with respect to the bay's tidal dynamics and its effect upon the flow field. Two cases, one with tidal current specification and the other with tidal level specification at the ocean–bay interface are presented here, and the relative merits of boundary conditions are discussed.

## MATHEMATICAL MODEL

The local thermodynamic and hydrodynamic state at any point in the fluid flow field can be determined by the solution of the set of local conservation equations describing the conservation of mass, momentum and energy. A constitutive relationship is also required in the usual form of an equation of state. The zeroth-order turbulent closure has been effected by using the eddy transport coefficient concept, which is analogous to a laminar fluid description with respect to the diffusion terms. The hydrostatic and Boussinesq approximation have been invoked. The horizontal eddy transport coefficient has been considered to be isotrophic and constant, and the vertical eddy transport coefficient, which is different from the horizontal coefficient, has also been considered constant.

Surface height variations at solid boundaries have been accounted for by specifying velocity slip conditions. This is justified, since the horizontal resolution of the numerical grid is not adequate to reproduce horizontal boundary layers. The Coriolis parameter has been assumed constant, considering the horizontal length scales involved. The free surface is considered to be isotropic and constant, and the vertical eddy transport coefficient, which is rigid-lid approximation as incorporated in a three-dimensional model by Sengupta and Lick[13] and later applied by Sengupta *et al.*[9] to South Biscayne Bay.

One of the problems associated with finite difference approximations, is the adequate representation of domain boundaries and bottom topography. The free surface and the variable bottom topography are specified in the model by following Phillips,[14] vertical stretching transformation of the vertical co-ordinate. This method has been used for the free surface model by Freeman *et al.*[15] This co-ordinate transformation is expressed as:

$$\alpha = x$$

$$\beta = y$$

$$\sigma = \frac{Z(x, y, z, t)}{H(x, y, t)} = \frac{Z + \eta(x, y, t)}{h(x, y) + \eta(x, y, t)} \tag{1}$$

where Appendix II gives the notation used throughout this paper. Figures 2 and 3 illustrate the free surface geometry in the unstretched and stretched co-ordinate systems, respectively.

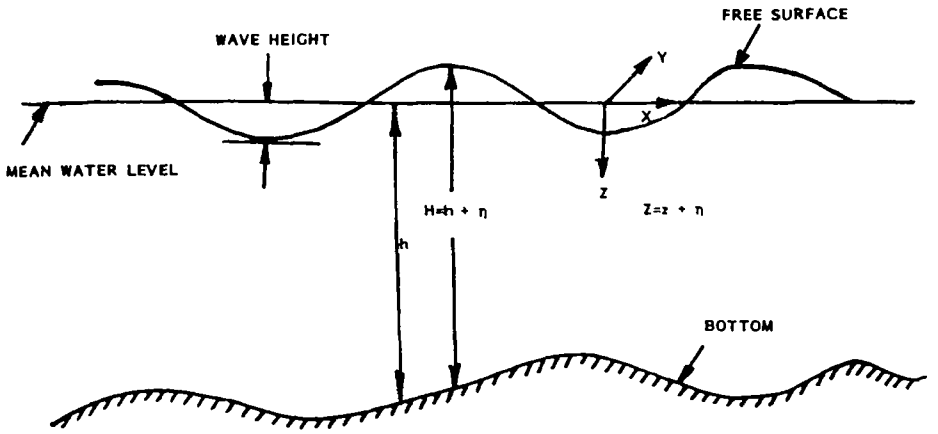


Figure 2. The xyz co-ordinate system for the free-surface model

Thus, the governing equations under the stated approximations, with vertical co-ordinate normalization with some small terms in horizontal diffusion neglected, and in the conservative form are expressed as follows:

*Governing equations*

Continuity equation:

$$\frac{\partial H}{\partial t}+\frac{\partial (Hu)}{\partial \alpha}+\frac{\partial (Hv)}{\partial \beta}+H\frac{\partial \Omega}{\partial \sigma}=0 \tag{2}$$

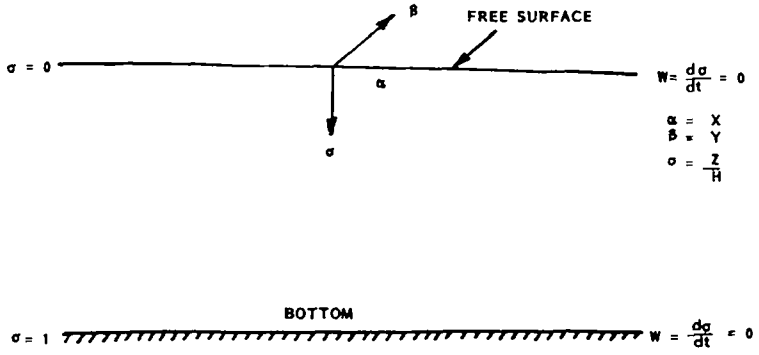


Figure 3. The αβσ co-ordinate system for the free-surface model

Momentum equations:

$$\frac{\partial(Hu)}{\partial t}+\frac{\partial(Huu)}{\partial\alpha}+\frac{\partial(Huv)}{\partial\beta}+H\frac{\partial(u\Omega)}{\partial\sigma}$$
$$=\left\{-\frac{1}{\rho}\left(\frac{\partial P}{\partial\alpha}\right)+g\left(\sigma+\frac{\partial H}{\partial\alpha}-\frac{\partial n}{\partial\alpha}\right)+fv\right\}$$
$$+K_H\left\{\frac{\partial}{\partial\alpha}\left(H-\frac{\partial u}{\partial\alpha}\right)\right\}+K_H\left\{\frac{\partial}{\partial\beta}\left(H-\frac{\partial u}{\partial\beta}\right)\right\}$$
$$+\frac{1}{\rho}\left\{\frac{1}{H}\frac{\partial}{\partial\sigma}\left(\rho K_v\frac{\partial u}{\partial\sigma}\right)\right\} \tag{3}$$

$$\frac{\partial(Hv)}{\partial t}+\frac{\partial(Huv)}{\partial\alpha}+\frac{\partial(Hvy)}{\partial\beta}+H\frac{\partial(v\Omega)}{\partial\sigma}$$
$$=H\left\{-\frac{1}{\rho}\left(\frac{\partial P}{\partial\beta}\right)+g\left(\sigma\frac{\partial H}{\partial\beta}-\frac{\partial\eta}{\partial\beta}\right)-fu\right\}$$
$$+K_H\left\{\frac{\partial}{\partial\alpha}\left(H\frac{\partial v}{\partial\alpha}\right)\right\}+K_H\left\{\frac{\partial}{\partial\beta}\left(H\frac{\partial v}{\partial\beta}\right)\right\}$$
$$+\frac{1}{\rho}\left\{\frac{1}{H}\frac{\partial}{\partial\sigma}\left\{\rho K_v\frac{\partial v}{\partial\sigma}\right)\right\} \tag{4}$$

Energy equation:

$$\frac{\partial(HT)}{\partial t}+\frac{\partial(HuT)}{\partial\alpha}+\frac{\partial(HvT)}{\partial\beta}+H\frac{\partial(\Omega T)}{\partial\sigma}$$
$$=B_H\left\{\frac{\partial}{\partial\alpha}\left(H\frac{\partial T}{\partial\alpha}\right)\right\}+B_H\left\{\frac{\partial}{\partial\beta}\left(H\frac{\partial T}{\partial\beta}\right)\right\}$$
$$+\frac{1}{\rho}\left\{\frac{1}{H}\frac{\partial}{\partial\sigma}\left(\rho B_v\frac{\partial T}{\partial\sigma}\right)\right\} \tag{5}$$

The vertical momentum equation has been replaced, via the hydrostatic approximation, by the hydrostatic equation:

$$P(\alpha,\beta,\sigma,t)=P(\alpha,\beta,\sigma=0,t)+gH\int_{\sigma=0}^{\sigma}\rho(\alpha,\beta,\sigma,t)\,d\sigma \tag{6}$$

where by the equation of state for the South Biscayne Bay, as given by Veziroglu *et al.*,[16] $\rho$ is given as:

$$\rho(\alpha,\beta,\sigma,t)=\rho(T)=1{\cdot}029431-0{\cdot}000020T-0{\cdot}0000048T^2 \tag{7}$$

Next, by following Freeman *et al.*[15], two vertically integrated forms of the continuity equation (2) are used in the model as follows:

Surface height equation:

$$\frac{\partial H}{\partial t}=-\int_{\sigma=0}^{1}\left\{\frac{\partial(Hu)}{\partial\alpha}+\frac{\partial(Hv)}{\partial\beta}\right\}d\sigma \tag{8}$$

Equivalent vertical velocity (in $\alpha, \beta, \sigma$):

$$\Omega = -\frac{1}{H}\int_{\sigma=0}^{\sigma}\left\{\frac{\partial(Hu)}{\partial\alpha}+\frac{\partial(Hv)}{\partial\beta}\right\}d\sigma + \frac{\sigma}{H}\int_{\sigma=0}^{1}\left\{\frac{\partial(Hu)}{\partial\alpha}+\frac{\partial(Hv)}{\partial\beta}\right\}d\sigma \tag{9}$$

The actual vertical velocity (in $x, y, z$) is related to $\Omega$ as follows:

$$W = \frac{dz}{dt} = H\Omega + \sigma\frac{dh}{dt} + (\sigma - 1)\frac{d\eta}{dt} \tag{10}$$

where

$$\Omega = \frac{d\sigma}{dt}$$

$$\frac{dh}{dt} = \frac{\partial h}{\partial t} + u\frac{\partial h}{\partial\alpha} + v\frac{\partial h}{\partial\beta}$$

$$\frac{d\eta}{dt} = \frac{\partial\eta}{\partial t} + u\frac{\partial\eta}{\partial\alpha} + v\frac{\partial\eta}{\partial\beta}$$

Equations (2)–(9) represent the system of governing equations for the dependent state variables $H, u, v, \Omega, P, \rho$ and $T$. The nature of these equations require the specification of initial and boundary conditions to complete the mathematical formulation for obtaining a unique, convergent solution for the local state of the fluid.

*Initial conditions*

The initial conditions have been prescribed as follows:

$$\eta(\alpha, \beta, 0) = H(\alpha, \beta, 0) - h(\alpha, \beta) = 0$$
$$u(\alpha, \beta, \sigma, 0) = v(\alpha, \beta, \sigma, 0) = \Omega(\alpha, \beta, \sigma, 0) = 0$$
$$T(\alpha, \beta, \sigma, 0) = T_0(\alpha, \beta, \sigma)$$
$$P(\alpha, \beta, \sigma, 0) = P_0(\alpha, \beta, \sigma)$$
$$\rho(\alpha, \beta, \sigma, 0) = \rho_0(\alpha, \beta, \sigma)$$

It is necessary to do this in order to ensure compatibility between $\eta$ and $u, v, \Omega$, initially. These quantities are taken equal to zero, since current measurements are not nearly as extensive as to provide an adequate representation of the initial velocity field. The initial free surface position $\eta(\alpha, \beta, 0)$ can be specified from an existing tide data base, but only when the initial velocity field is simultaneously known. The initial temperature field is specified by utilizing an infrared thermal scanner data base for surface temperature taken on 15 April 1975 and presented in Veziroglu *et al.*[16] The vertical variation in temperature is considered negligible, initially since the bay is shallow and well mixed by vertical turbulent diffusion.

*Boundary conditions*

The boundary conditions have been prescribed as follows:

| *At the surface,* $\sigma = 0$ | *At the bottom,* $\sigma = 1$ |
|---|---|
| $\Omega = 0$ | $\Omega = 0$ |
| $\frac{\partial u}{\partial \sigma} = -\left(\frac{H}{\rho K_v}\right)\tau_{zx}$ | $u = 0$ |
| $\frac{\partial v}{\partial \sigma} = -\left(\frac{H}{\rho K_v}\right)\tau_{zy}$ | $v = 0$ |
| $\frac{\partial T}{\partial \sigma} = -\left(\frac{HK_s}{\rho C_p B_v}\right)(T_e - T_s)$ | $\frac{\partial T}{\partial \sigma} = 0$ |

*At lateral solid boundaries*

| *On x-boundaries* | *On y-boundaries* |
|---|---|
| $u = 0$ | $\frac{\partial (Hu)}{\partial \beta} = 0$ |
| $\frac{\partial (Hv)}{\partial \alpha} = 0$ | $v = 0$ |
| $\frac{\partial T}{\partial \alpha} = 0$ | $\frac{\partial T}{\partial \beta} = 0$ |

*At lateral open boundaries*

| *At the ocean–bay interface* | *At the outlet* |
|---|---|
| $u = 0$ | $u = 0$ |
| $v = v_0(t)$ or $\eta = \eta_0(t)$ | $\frac{\partial v}{\partial \beta} = 0$ |
| $\frac{\partial v}{\partial \beta} = 0$ {for $\eta = \eta_0(t)$} | $\frac{\partial T}{\partial \beta} = 0$ |
| $\frac{\partial T}{\partial \beta} = 0$ | |

Either the tidal current velocity, $V_0(t)$, or the tide level variation, $\eta_0(t)$, can in general be specified as the forcing function at the ocean–bay interface, i.e.

$$\eta = \eta_0(t) \tag{11}$$

or,

$$v = v_0(t) \tag{12}$$

The first case being for tide level specification, which is obtained from an existing tide data base taken from Schneider.[10] The second case is for tidal current velocity specification, which unless measured directly requires an additional assumption about the nature of the inlet (ocean–bay interface) with respect to the bay geometry. Appendix I shows how $V_0(t)$ is

determined through approximations and is specified for the South Biscayne Bay. Note, both boundary conditions at the inlet yield well-behaved, stable and convergent numerical solutions.

## METHOD OF SOLUTION

### *Grid system*

The system of governing equations together with the initial and boundary conditions are cast into finite difference form employing an explicit scheme. A three-dimensional numerical grid system in $\alpha, \beta, \sigma$ co-ordinates is established whereby the grid nodes are enumerated by the indices $I, J, K$, respectively. The numerical grid system used for this study of the South Biscayne Bay is shown in Figure 4.

### *Solution algorithm*

Roache[17] discusses numerical techniques for viscous flow problems. Alternating direction implicit techniques allow the largest time steps while avoiding iterative procedures inherent in other implicit techniques. However, for non-rectangular domains the programming difficulties are prohibitive. Therefore, explicit finite difference schemes are most suited to problems in multi-dimensional irregular boundary domains. The schemes are summarized in Table I. The procedure of computation follows the sequence listed below.

1. Compute surface height, $H^{(n+1)}$
2. Compute velocities $(u, v)^{(n+1)}$
3. Compute $\Omega^{n+1}$
4. Compute $T^{n+1}$
5. Compute $\rho^{n+1}$
6. Compute $P^{n+1}$

This procedure is repeated at each time step. The initial step uses forward difference in time followed by central difference in subsequent time steps.

The appropriate numerical stability criteria are the Courant–Freidrichs–Lewy (CFL) condition for surface gravity waves, the convective criteria, the diffusive criteria, and the Coriolis criteria. For the South Biscayne Bay the vertical diffusion criteria is the most restrictive. Thus, a rigid-lid approximation would not provide any computational advantage

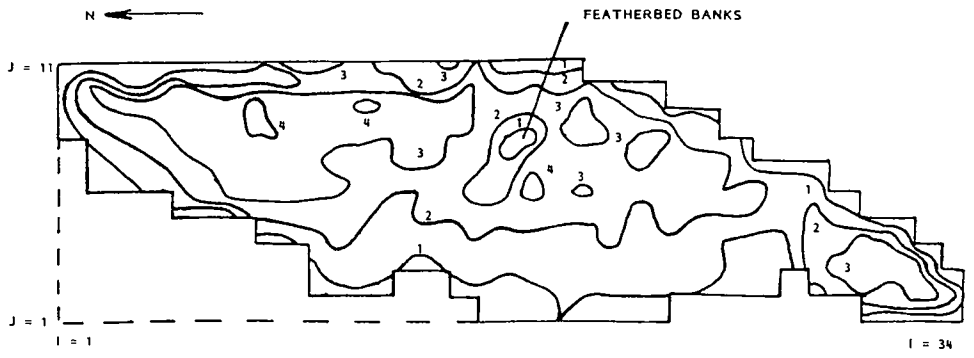


Figure 4. Grid system and bottom topography in metres

Table I

| Initial step | Subsequent step |
|---|---|
| $H^{n+1} = H^n + f(u^n, v^n, H^n)\,\Delta t$ | $H^{n+1} = H^{n-1} + f(u^n, v^n, H^n)\,2\Delta t$ |
| $(Hu)^{n+1} = (Hu)^n + f(H^n, u^n, v^n, P^n, \rho^n, \Omega^n)\,\Delta t$ | $(Hu)^{n+1} = (Hu)^{n-1} + (\text{Coriolis})^n$, $(\text{pressure})^n$ $(\text{inertia})^n$, $(\text{horizontal diffusion})^{n-1}$, $(\text{vertical diffusion, DuFort–Frankel})^{n,n+1,n-1}_{2\Delta t}$ |
| Same for $v$-momentum | Same for $v$-momentum |
| $\Omega^{n+1} = f(H^{n+1}, u^{n+1}, v^{n+1})$ | Same as for initial step |
| $(HT)^{n+1} = (HT)^n + f(H^n, T^n, u^{n+1}, v^{n+1}, \rho^n, \Omega^{n+1})\,\Delta t$ | Same as for initial step |

for a relatively shallow estuary. Figure 4 shows the depths with respect to the mean water level for the South Biscayne Bay.

Other numerical approximations have been made in order to obtain stable numerical solutions, and, also, to decrease the computation time significantly. These approximations are given as follows:

1. Following Roache[17] adiabatic lateral boundary conditions are specified as:

$$T_w = T_{w+1} \text{ on } \sigma\text{-planes} \tag{13}$$

where $T_w$, the lateral boundary temperature, is equated to the adjacent interior grid temperature, $T_{w+1}$, after the value at the interior point has been calculated. For a shallow, vertically well-mixed bay this boundary condition is justifiable, since $\dfrac{\partial T}{\partial \sigma}$ is small and horizontal gradients of $H$ and $\eta$ are small. Note,

$$\frac{\partial T}{\partial x} = \frac{\partial T}{\partial \alpha} + \frac{\partial T}{\partial \sigma}\left(\frac{1}{H}\frac{\partial \eta}{\partial \alpha} - \frac{\sigma}{H}\frac{\partial H}{\partial \alpha}\right).$$

2. The outlet boundary condition $\dfrac{\partial v}{\partial \beta} = 0$ has been approximated as:

$$V_{\text{outlet}} = V_{\text{interior (adjacent point)}} \text{ on } \sigma\text{-planes} \tag{14}$$

This approximation has a truncation error on the order of $\Delta\beta$.

3. The inlet boundary condition for the case of $\eta = \eta_0(t)$, i.e. $\dfrac{\partial v}{\partial \beta} = 0$ is approximated as:

$$V_{\text{inlet}} = \bar{V}_{\text{interior (adjacent point)}} \text{ on } \sigma\text{-planes} \tag{15}$$

where

$$\bar{V}_{\text{interior}} = \sum_{I=7}^{16} V_{\text{interior}}/10$$

This numerical approximation was used, since $\eta_0(t)$ at the inlet is specified as constant in the interval $7 \le I \le 16$. More realistically, there will be spatial gradients of $\eta_0(t)$ along the inlet, due to the effects of wind shear and variable bottom topography. However, only one tide

gauge station provided the inlet tide level variation $\eta_0(t)$. Therefore, spatial variations in tide level could not be specified at this open boundary (ocean–bay interface) without additional field data.

## APPLICATION TO SOUTH BISCAYNE BAY

Figure 1 shows a map of the South Biscayne Bay. The bay is approximately 45 km long and 16 km wide. It has several basins connected by shallow limestone sills. The bay is isolated from the Atlantic Ocean by a series of keys. The major ocean exchange occurs through the safety valve region between Key Biscayne and Soldier Key. The safety valve region is about 14 km long with shallow linestone sills 1–3 km wide. There are approximately 20 channels in this area with a maximum depth of 5 m. The lower part of the bay has a number of creeks open to the ocean. The maximum depth in the bay is 4 m. The Featherbed Banks are a shallow region dividing the bay.

The boundaries of the bay system are schematized to fit on a grid 34 by 11 points, in the horizontal plane, and 5 points in the vertical direction. Figure 4 shows the horizontal grid system, and the depth contours. By vertical stretching the basin is transformed to constant depth and, hence, the 5 layers are equally spaced in this three-dimensional computational grid system. For the numerical simulations, the horizontal grid sizes are $\Delta x = \Delta y = \Delta\alpha = \Delta\beta = 1{\cdot}6$ km.

The numerical model as discussed thus far was run based on field data acquired on 15 April 1975 as presented by Veziroglu *et al.*[16] Table II gives the physical and meteorological data for this day. The model was run from 0800 EST to 2000 EST, with the air temperature and wind conditions specified every hour. The tidal input forcing function, both for the case of specifying tide level variation at the inlet, and for the other case of specifying tidal current velocity variation at the inlet, was included as a continuous sinusoidal time variation. The sinusoidal time variation of tide level at the inlet was obtained from a tide data base given by Schneider,[10] with high tide occurring 1000 EST for 15 April 1975. The tidal period was computed to be 1215 hours for this day.

Table II

| Time (EST) | Wind (m/sec)(mph) | $\tau zx$* | $\tau zy$ | $T_e$(°C)† | $K_s$(Cal/sec, cm$^2$°C)† |
|---|---|---|---|---|---|
| 0800 | 4·11(9·2)SSW | −0·37 | 0·15 | 31·7 | 0·00129 |
| 0900 | 6·17(13·8)SSW | −0·92 | 0·38 | 31·5 | 0·00179 |
| 1000 | 5·68(12·7)SSW | −0·74 | 0·30 | 32·9 | 0·00166 |
| 1100 | 6·71(15)S | −1·20 | 0·0 | 33·7 | 0·00201 |
| 1200 | 8·22(18·4)S | −2·20 | 0·0 | 34·5 | 0·00279 |
| 1300 | 8·22(18·4)S | −2·20 | 0·0 | 36·0 | 0·00279 |
| 1400 | 4·65(10·4)SSW | −0·45 | 0·19 | 37·0 | 0·00175 |
| 1500 | 4·11(9·2)WNW | 0·15 | 0·37 | 37·2 | 0·00130 |
| 1600 | 3·62(8·1)WNW | 0·11 | 0·28 | 37·2 | 0·00136 |
| 1700 | 3·62(8·1)WNW | 0·11 | 0·28 | 36·3 | 0·00121 |
| 1800 | 5·68(12·7)NW | 0·57 | 0·57 | 33·8 | 0·00173 |
| 1900 | 3·08(6·9)WNW | 0·08 | 0·18 | 35·0 | 0·00108 |
| 2000 | 4·65(10·4)WNW | 0·19 | 0·46 | 32·6 | 0·00149 |

* The wind shear stresses (in Dyn/cm$^2$) were computed based on the work of Wilson.[18]
† Values calculated using methods outlined by Edinger and Geyer[19] and Harleman–Stolzenbach.[20]

## RESULTS AND DISCUSSION

The numerical results based upon exciting the model for the prescribed data base, as discussed in the previous section for 15 April 1975, are presented for the two boundary conditions cases with specification of $V_0(t)$ and $\eta_0(t)$, respectively. The simulated results for these two cases are compared with each other, and comparisons with existing data bases are made.

Each case was run on a UNIVAC 1100/8 digital computer at the University of Miami. These two cases were run for a period of 12 h, that is, for one complete tidal cycle in order that initial transient numerical effects be small in final model results. First, however, a number of calibration runs were executed in order to adjust the eddy transport coefficients, and, also, to investigate systematically the boundary conditions for a realistic representation of the phenomenon.

*Case* I. $V_0(t)$ *specified at the ocean–bay inerface*

(a) *Phase relationships.* A sinusoidal tidal current velocity at the ocean exchange was specified. Figure 5 shows that a phase shift of approximately 3 h is observed between imposed velocity ($V_0(t)$) and produced surface heights ($\eta_0(t)$). This is close to the 90-degree phase shift assumed in calculating the velocity input (Appendix I).

Figure 6 shows the $u$-velocity and surface height at location ($I = 8$, $J = 8$) which is near the bay–ocean interface. The velocities are in general smallest for high and low tide, however, simple phase relationships are not apparent. It is observed that surface velocities can be in opposite direction to velocities at lower depths. Figure 7 shows similar plots for ($I = 27$, $J = 5$) a location far removed from the inlet, close to the southern end of the domain. Here the velocities are in phase. The lowest velocities are for minimum of maximum values of surface height.

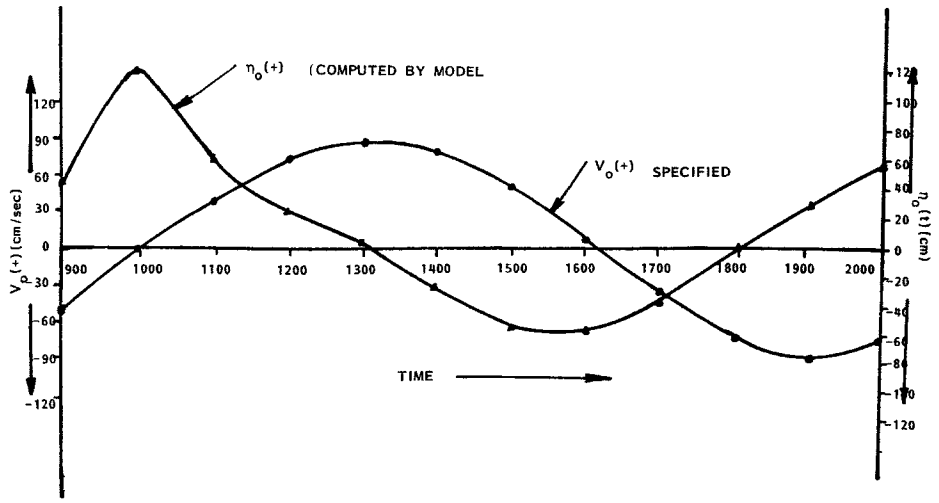


Figure 5. Surface height and imposed velocity at ($I = 10$) ocean–bay interface Case I

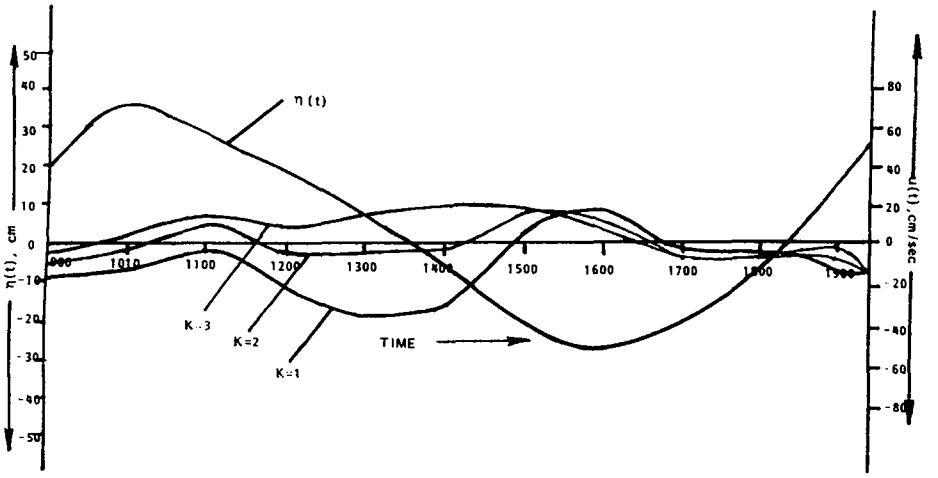


Figure 6. Variation of surface height and $u$-velocity at location ($I = 8$, $J = 8$) Case I

Figures 8 and 9 show predicted surface height and averaged measured height at Coconut Grove (Station 2) and Elliot Key (Station 6) respectively. The comparison at the first location has a deviation of approximately 100 per cent in magnitude and 1·5 h in phase. At the second location the errors are dismal. The data was taken for Schneider's tide gauge Stations 2, and 6, shown in Figure 1. The deterioration of simulation at Elliot Key may be due to the effect of phase differences in forcing tidal boundary condition at the shoals and the creeks. Also, Station 6 is close enough to the creeks to be directly influenced by ocean driving forces through the creeks.

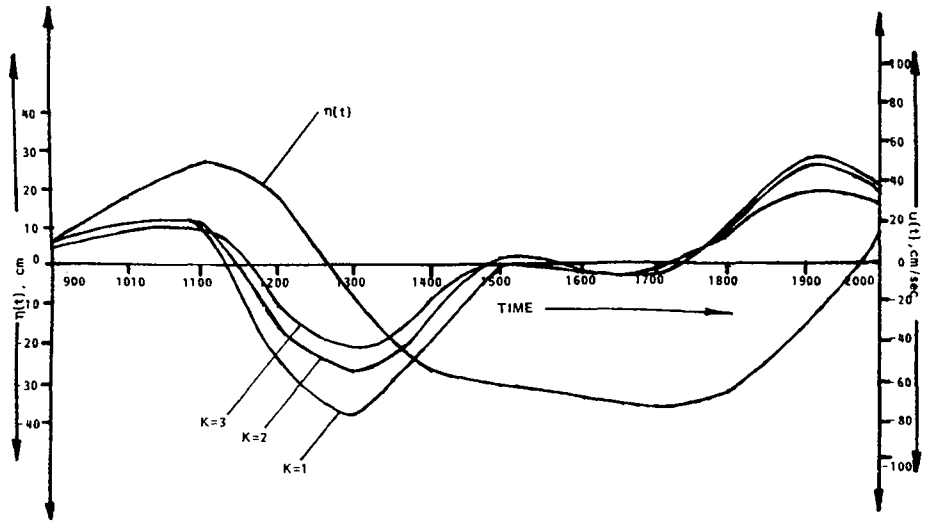


Figure 7. Variation of surface height and $u$-velocity at location ($I = 27$, $J = 5$) Case I

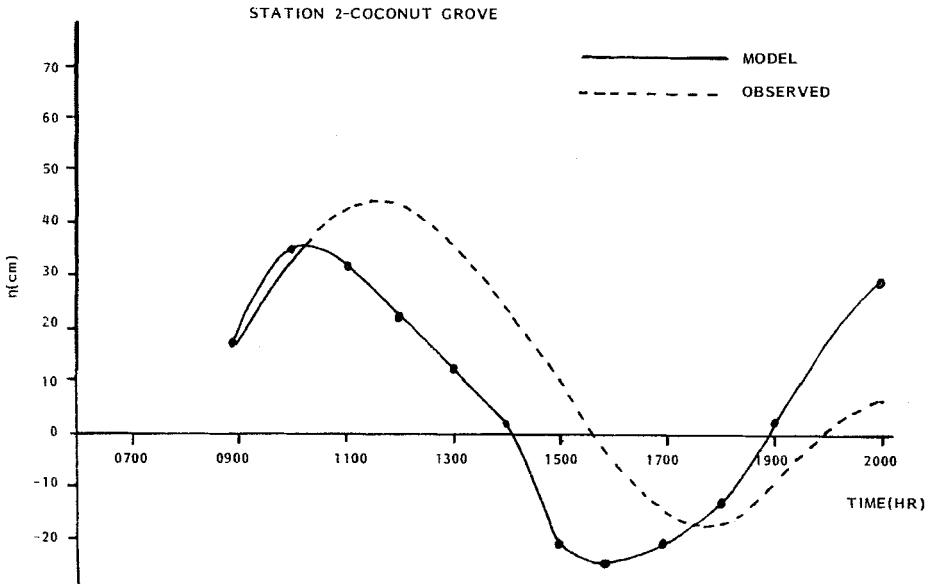


Figure 8. Predicted and measured values of surface height at Coconut Grove ($I = 4$, $J = 6$) Case I

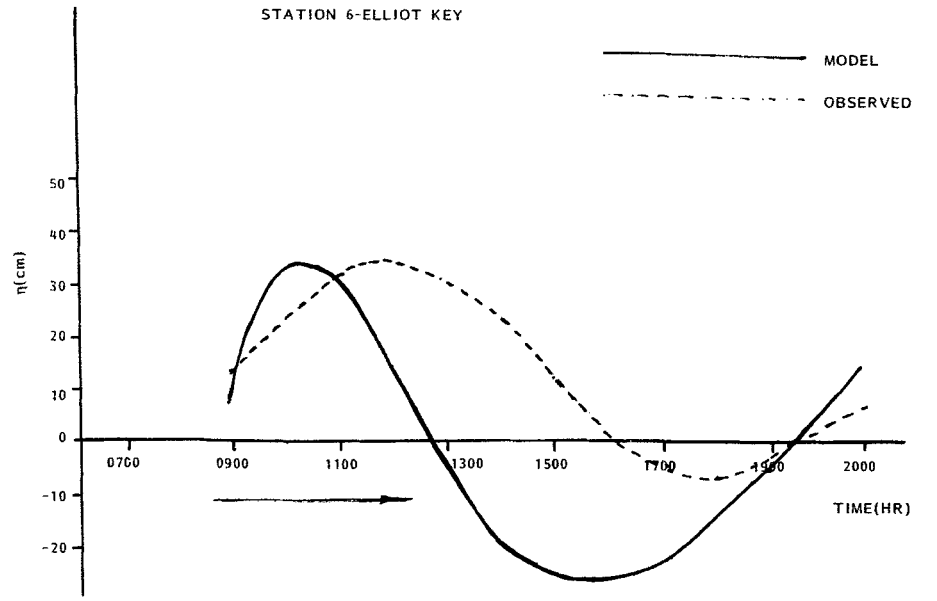


Figure 9. Predicted and measured values of surface height at Elliot Key ($I = 21$, $J = 10$) Case I

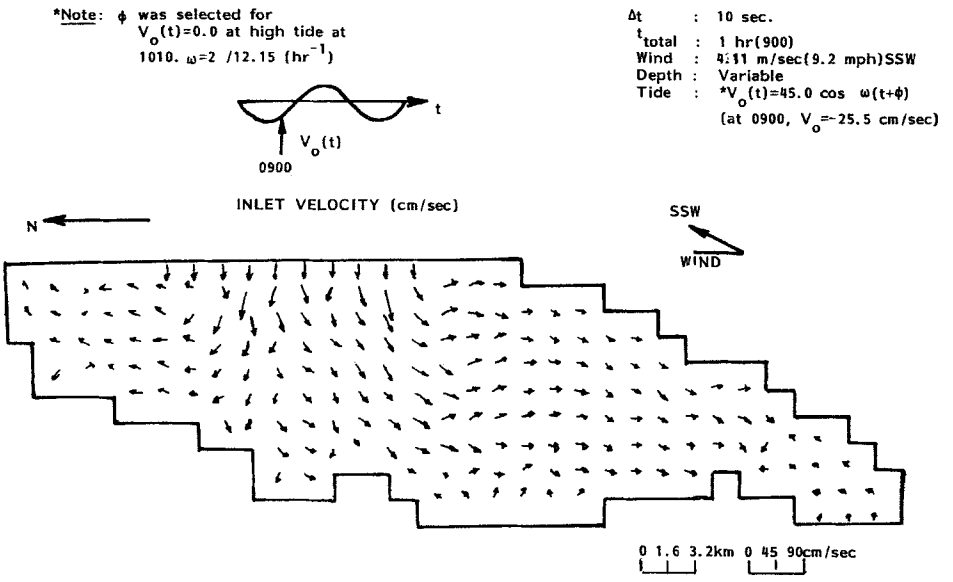


Figure 10. Surface velocity distribution for Biscayne Bay at 0900 EST; 15 April 1975, Case I

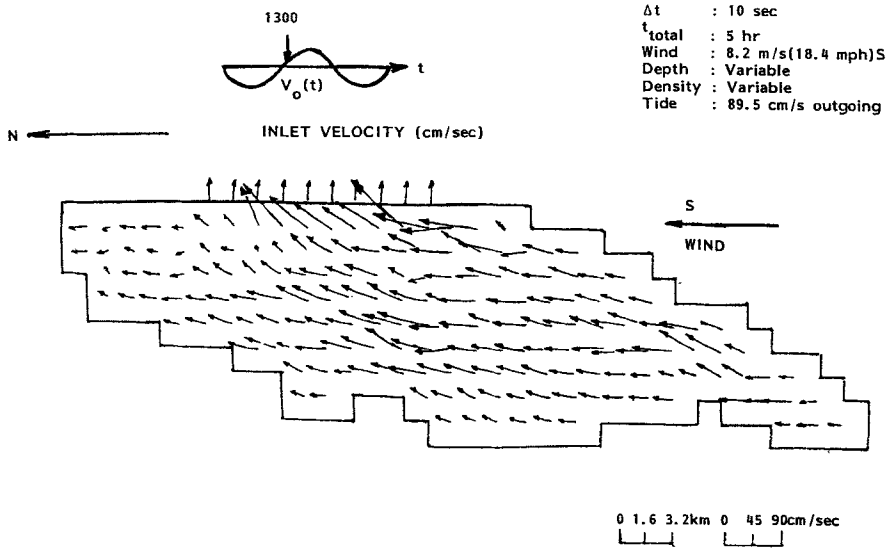


Figure 11. Computed horizontal velocity pattern at surface of Biscayne Bay, 1300 EST, 15 April 1975, Case I

(b) *Velocity field.* The simulation started at 0800 EST. Initially the surface is flat and the velocities are zero. Figure 10 shows the surface velocities at 0900 EST. The general pattern of circulation shows a bifurcation of the incoming flow to the north and south of the bay. Some of the velocities at adjacent grid nodes to the inlet are higher than the specified inlet velocities. This is caused by a topographical constriction in the vertical direction. The flows at the south end of the bay are in the direction of the wind indicating that effects of tidal input have not yet been felt. The northerly flows in the north end are somewhat enhanced by the wind. Figures 11 and 12 show surface velocities with outgoing (1300 EST) and incoming

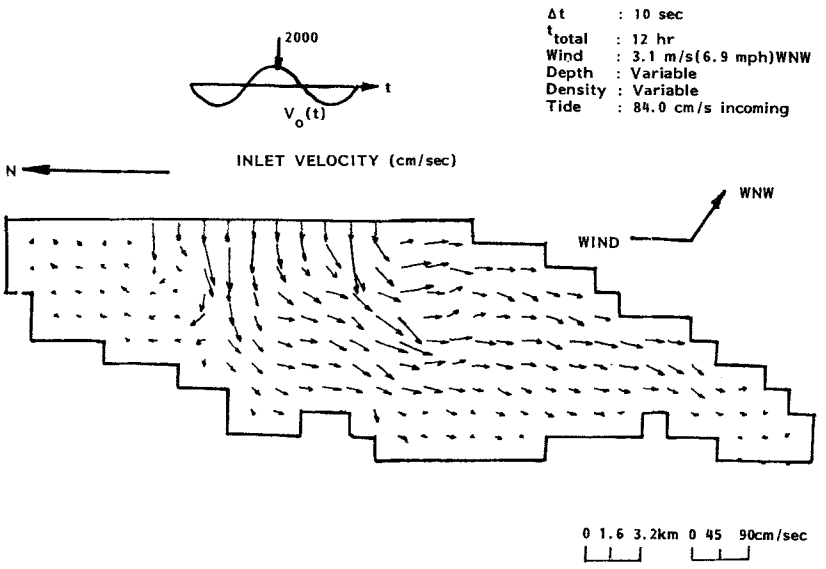


Figure 12. Computed horizontal velocity pattern at surface of Biscayne Bay, 2000 EST, 15 April 1975, free surface model.

(2000 EST) flows respectively, at the ocean–bay interface. Figure 11 indicates a general flow pattern towards the outlet. Northerly flow at the northern part of the bay is attributable to the wind from the south. The circulation pattern at 2000 EST is similar to 0900 EST except for minor modification owing to winds and the minimal effect of initial conditions at 2000 EST.

(c) *Temperature field.* The temperature field was intialized at 1000 EST using IR data obtained by airborne sensors. The data was corrected using ground truth measurements from boats. It was assumed that the domain was vertically well mixed. Figure 13 shows a comparison of measured and predicted isotherms at 1400 EST. It should be noted that the IR data is not synoptic since several flights are needed to cover the bay. There is about 1·5 h lag between data collected near the mainland with data over the key. The total variation of temperature between measured and predicted values is about 2°C. Qualitative behavior such as heating near shore and at Featherbed banks is simulated reasonably well.

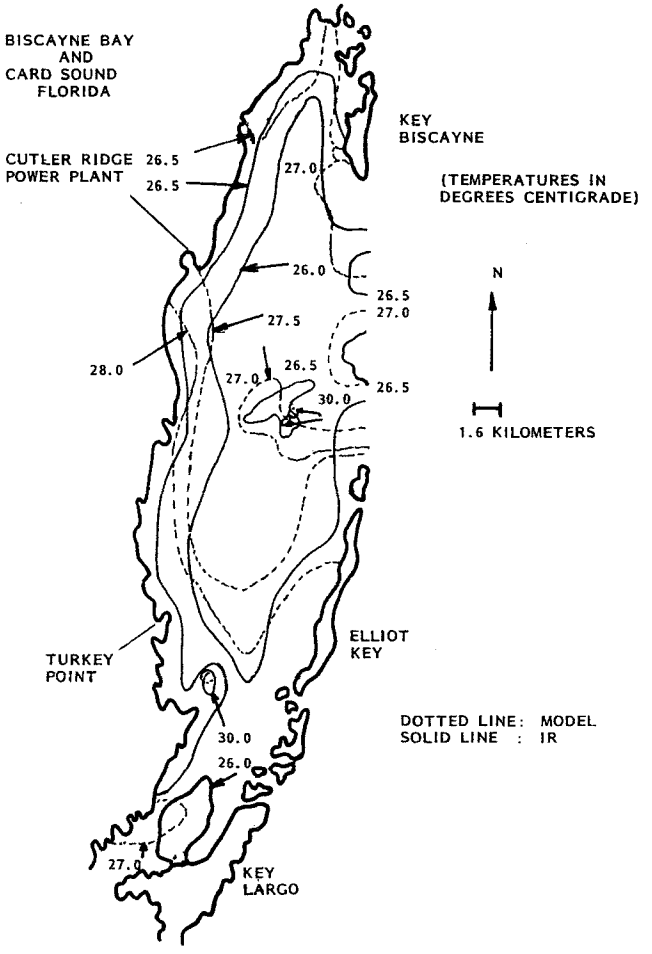


Figure 13. Comparison of IR data with free surface model results (15 April 1975) at 1400 EST, Case I

*Case* II. $\eta_0(t)$ *specified at the ocean–bay interface*

(a) *Phase relationships.* Surface height variation at the inlet, $\eta_0(t)$, was specified from Schneider's data at Station 1 at Miami Beach. Figure 14 shows the imposed value of $\eta_0(t)$ and predicted velocities $V_0(t)$ at the inlet. The phase lag is 4·8 h. A three-hour difference would correspond to a 90-degree phase relationship. Therefore, the assumption of a 90-degree phase relationship between $V_0(t)$ and $\eta_0(t)$ used to calculate $V_0(t)$ specification for Case I is inaccurate.

Figures 15 and 16 show the time variation of surface height and $u$-velocity near the ocean–bay interface and south end of the bay, respectively. It is seen that near the inlet, velocities at the surface and lower depths may be in opposite directions during part of the tidal cycle. Away from the inlet the velocities with depth are in phase. Maximum and

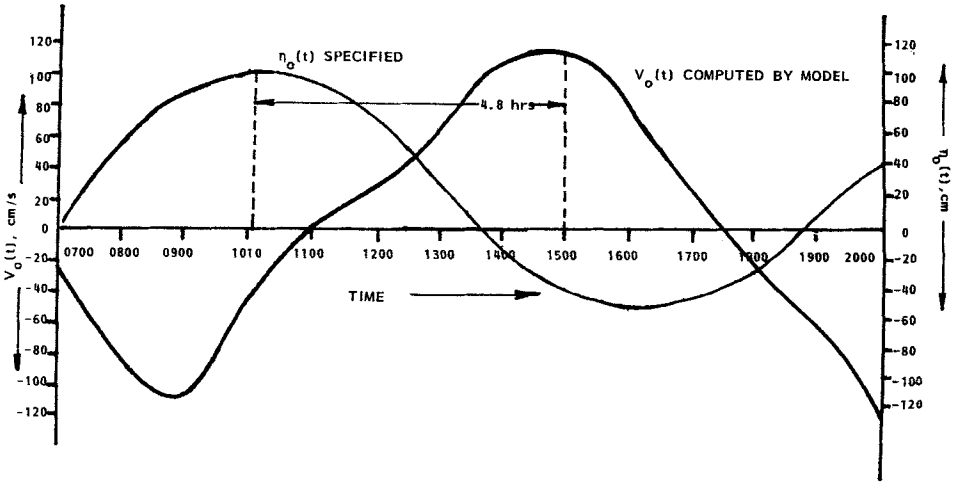


Figure 14. Predicted velocity and imposed surface height at ($I = 10$) ocean–bay interface, Case II

minimum values of surface height approximately correspond to minimum values of velocity. The surface height variations at ($I = 27$, $J = 5$) are approximately two hours delayed compared to ($I = 8$, $J = 8$).

Figures 17 and 18 present observed versus computed tide levels at Coconut Grove and Elliot Key, respectively. After initial transient effects, the agreement in magnitude and phase is good. The phase errors at Elliot Key are larger than at Coconut Grove. The effects of neglected driving forces at the creeks could be a possible explanation for the relative difference in errors at the two locations. It should be noted that Schneider's data was yearly averaged, whereas the simulations are for a particular day with wind effects included.

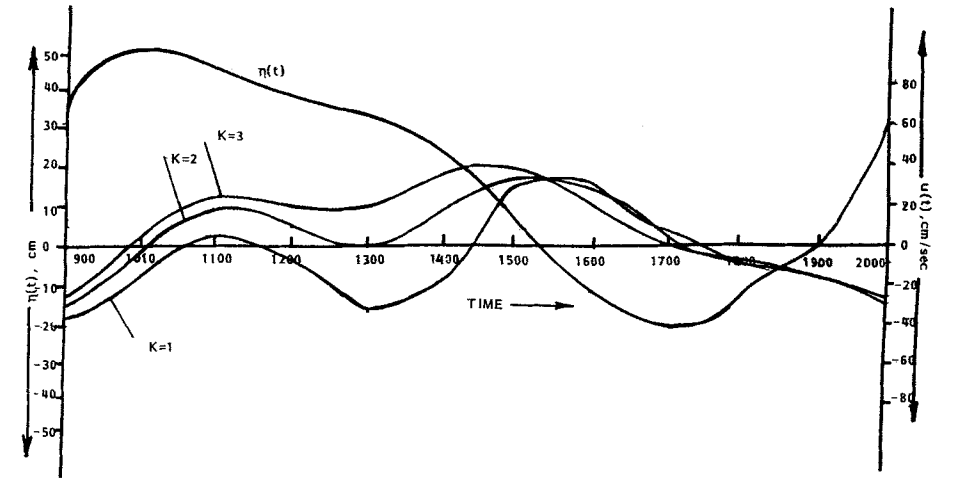


Figure 15. Variation of surface height and $u$-velocity at location ($I = 8$, $J = 8$), Case II

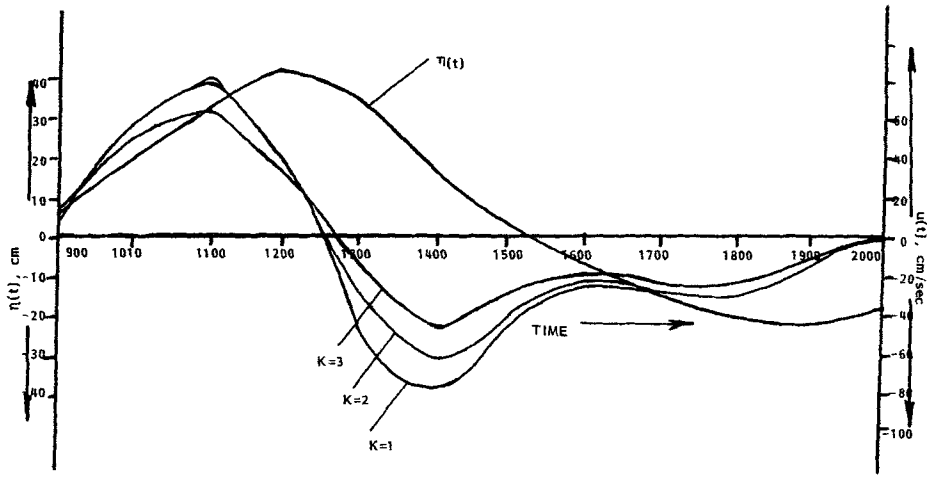


Figure 16. Variation of surface height and $u$-velocity at location ($I = 27$, $J = 5$), Case II

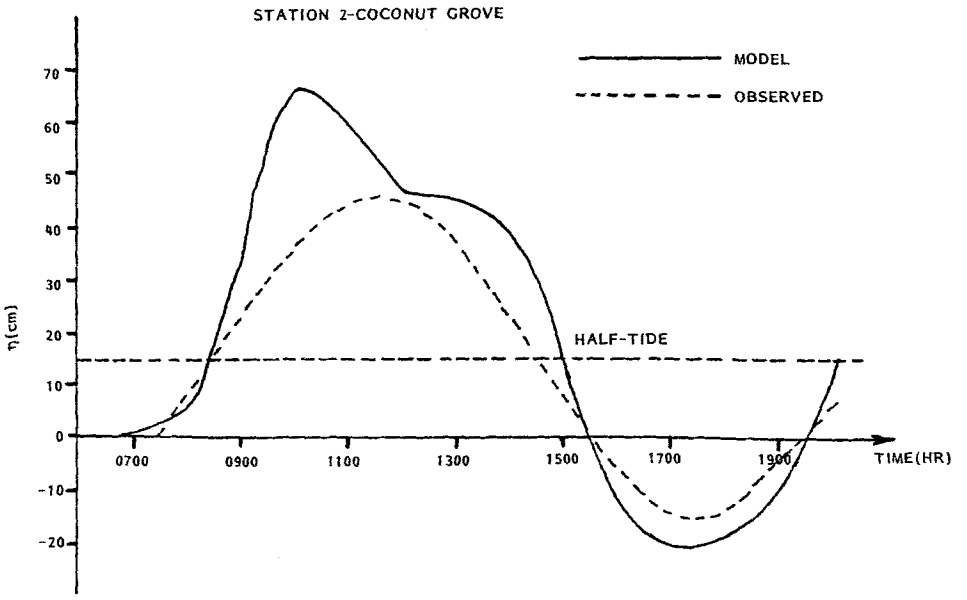


Figure 17. Predicted and measured values of surface height at Coconut Grove ($I = 4$, $J = 6$), Case II

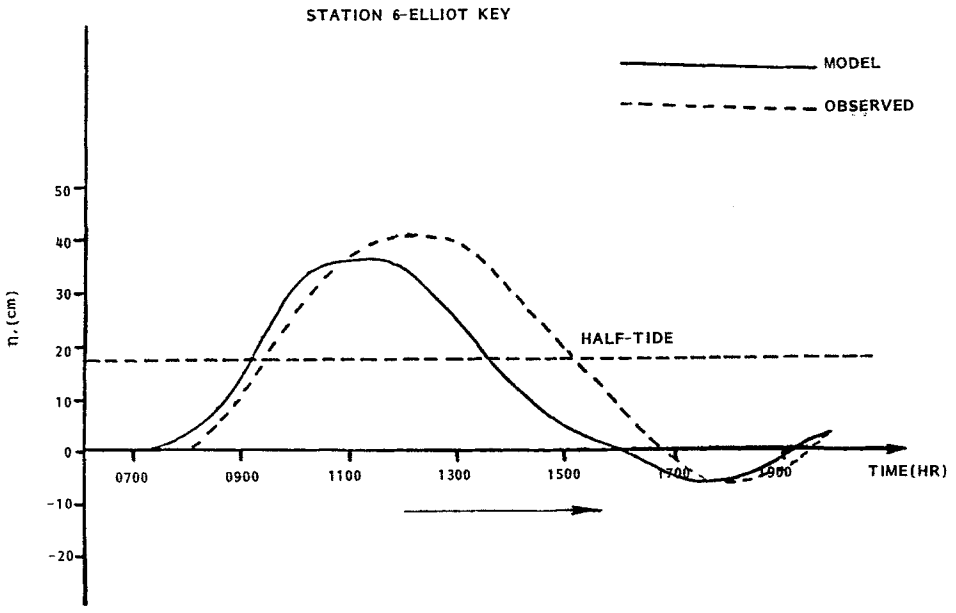


Figure 18. Predicted and measured values of surface height at Elliot Key ($I = 21$, $J = 10$), Case II

(b) *Velocity field.* This simulation was started at 0630 EST when $\eta_0(t) = 0$ and thus the initial conditions were a flat surface with zero velocities. Figures 19, 20 and 21 show the velocity fields at 0900 EST, 1300 EST and 2000 EST, respectively. The circulation patterns are very similar to the $V_0(t)$ specification case. Though the gross features are the same, the differences in details are observed in the phase relationship discussion.

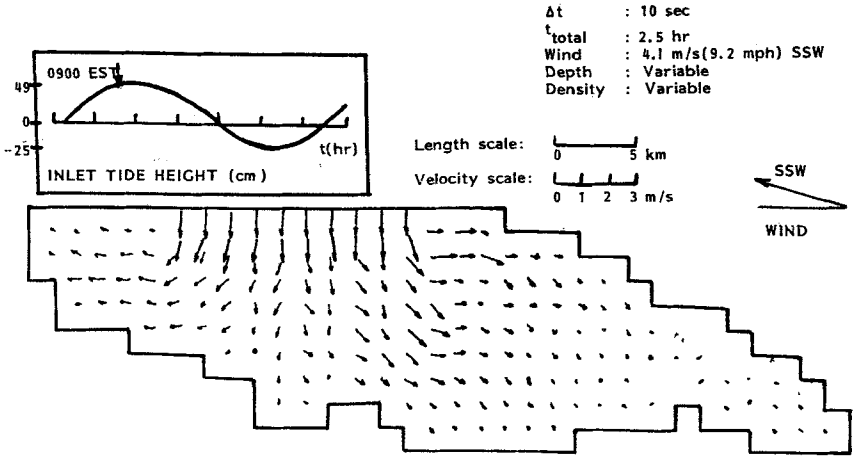


Figure 19. Computed horizontal velocity pattern at surface of Biscayne Bay, 0900 EST, 15 April 1975, Case II

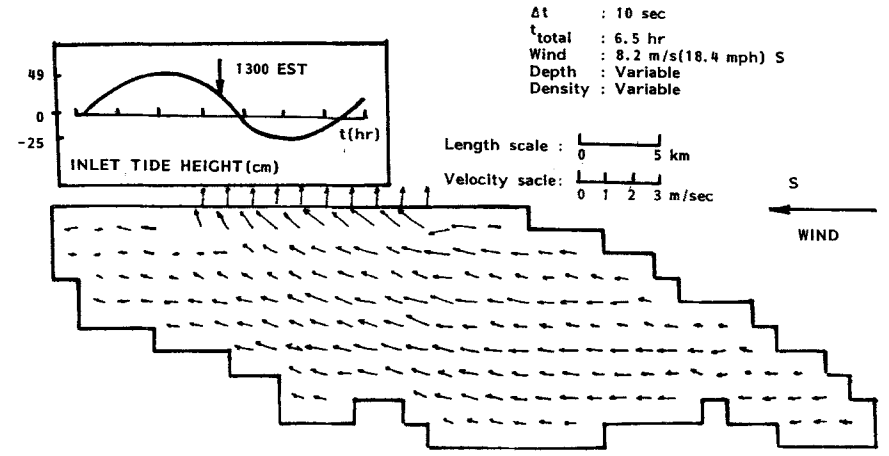


Figure 20. Computed horizontal velocity pattern at surface of Biscayne Bay, 1300 EST, 15 April 1975, Case II

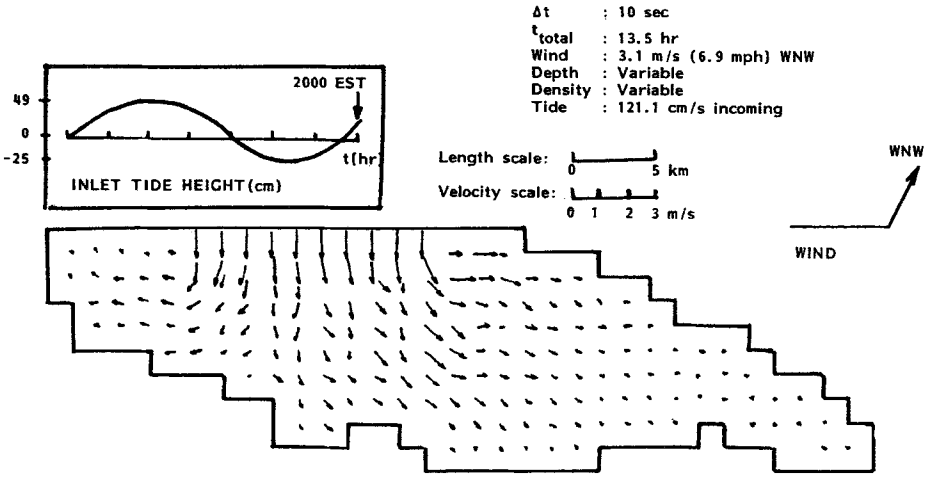


Figure 21. Computed horizontal velocity pattern at surface of Biscayne Bay, 2000 EST, 15 April 1975, Case II

(c) *Temperature field.* Figure 22 shows the comparison of IR data with simulated results for 1400 EST. It can be seen that the major features are well reproduced and agreement is within 1°C. Hence, the $\eta_0(t)$ specification is also responsible for better prediction of thermal behavior than the $V_0(t)$ specification at the open boundary.

## CONCLUSIONS

1. This simulation for a shallow estuary indicates that three-dimensional features are present in the flow pattern, including flow reversal. It is expected that inclusion of buoyancy

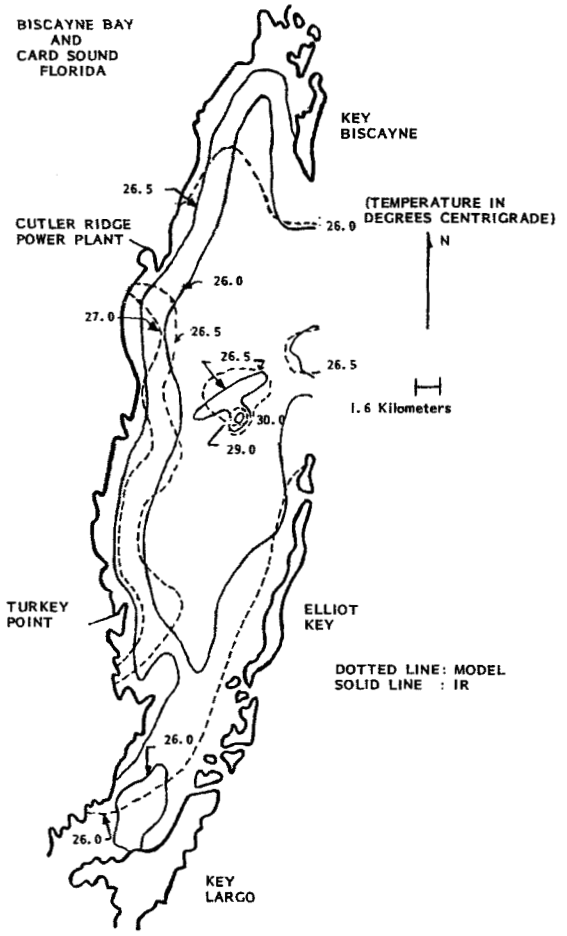


Figure 22. Comparison of IR data with free surface model results (15 April 1975) at 1400 EST, Case II

effects would enhance three-dimensional behavior. Thus, two-dimensional models, while economical, may be inadequate for simulating details of flow structure and pollutant dispersal.

2. Specification of boundary conditions at ocean–estuary interface has a significant effect on simulations. While general circulation patterns were the same for $V_0(t)$ and $\eta_0(t)$ specifications, major differences in details of circulation and phase relationship were present.

3. The specification of $\eta_0(t)$ was demonstrably better in predicting surface heights and their phases at different parts of the bay. It is also resulted in considerably better agreement between measured and simulated temperature distributions.

4. It is concluded that specification of $\eta_0(t)$ at the ocean–bay interface should be used even when detailed variations along the interface are not known.

## APPENDIX I. INLET TIDAL CURRENT VELOCITY

The inlet tidal current velocity variation, $V_0(t)$, can be obtained from the measured inlet tide level variation, $\eta_0(t)$, as follows. Ippen[21] has shown, by using a one-dimensional analysis, that the current and surface elevation variations in a channel open at one end and closed at the other can result in a standing wave, whereby $\eta_0(t)$ and $V_0(t)$ are 90 degrees out of phase. This 90-degree phase relationship has been assumed in calculating $V_0(t)$, by assuming that the surface waves traversing the width of the bay (from the inlet to the opposite westbank shore) are reflected and, thus, set up a standing wave. $\eta_0(t)$ and $V_0(t)$ for a standing wave in one-dimensional are expressed as,

$$\eta(t) = 2\eta_{max} \cos \omega t \cos k\beta \tag{16}$$

and,

$$V(t) = 2\frac{\eta_{max}}{h} C_0 \sin \omega t \sin k\beta \tag{17}$$

where

$\eta_{max}$ = the amplitude of the measured tide level variation at the inlet
$h$ = the average depth along the inlet
$\beta$ = the co-ordinate normal to the inlet
$C_0 = \sqrt{(gh)}$, the phase velocity of the tidal wave for shallow water
$\omega$ = the angular frequency of the tidal wave
$k$ = the wave number of the tidal wve

at the westbank opposite the inlet (closed end), $\beta = 0$, following the co-ordinate system used by Ippen. Hence, equations (16) and (17) become,

$$\eta(\beta = 0) = 2\eta_{max} \cos \omega t \tag{18}$$

$$V(\beta = 0) = 0 \tag{19}$$

At the inlet (open end), $\beta = l$, where $l$ = the width of the bay between the inlet and the westbank. Hence, equations (16) and (17) become,

$$\eta(\beta = l) = 2\eta_{max} \cos \omega t \cos kl \tag{20}$$

$$V(\beta = l) = 2\frac{\eta_{max}}{h} c_0 \sin \omega t \sin kl \tag{21}$$

However, as will be shown below for the South Biscayne Bay

$$l \ll \lambda \tag{22}$$

where $k = 2\pi/\lambda$, $\lambda$ = the wavelength of the tidal wave. Using this fact, equations (20) and (21) reduce to,

$$\eta_0(t) = \eta(\beta = \rho) = 2\eta_{max} \cos \omega t \tag{23}$$

$$V_0(t) = V(\beta = l) = \frac{2\eta_{max} C_0}{h} \frac{2\pi l}{\lambda} \sin \omega t \tag{24}$$

where for $l \ll \lambda$,

$$\cos \frac{2\pi l}{\lambda} = 0$$

$$\sin \frac{2\pi l}{\lambda} = \frac{2\pi l}{\lambda}$$

Thus, equation (24) was used to calculate $V_0(t)$ from the measured tide level variation at the inlet, by assuming a 90-degree phase relation between $\eta_0(t)$ and $V_0(t)$.

Now, for the present case the above variables were given the following numerical values.

$$C_0 = \sqrt{(gh)} = \sqrt{(980 \times 190)} = 4{\cdot}3 \times 10^2 \text{ cm/sec}$$

$$C_0 = \frac{\omega}{k} = \frac{2\pi/T}{2\pi/\lambda} = \frac{\lambda}{12} \quad \text{where} \quad T = 12 \text{ h}$$

and,

$$\lambda = 12C_0 = 1{\cdot}86 \times 10^7 \text{ cm}$$
$$l = 10\Delta\beta = 1{\cdot}6 \times 10^6 \text{ cm}$$
$$\eta_{max} = 37{\cdot}0 \text{ cm}$$
$$h = 190{\cdot}0 \text{ cm}$$

So that,

$$2\pi l/\lambda = 0{\cdot}54 \quad \text{and} \quad l/\lambda = 0{\cdot}09 \ll 1$$

and, finally,

$$V_0(t) = \frac{(2{\cdot}0)(37{\cdot}0)(4{\cdot}3 \times 10^2)}{(190{\cdot}0)} (0{\cdot}54) \sin \omega t$$
$$\simeq (90{\cdot}0) \sin \omega t \tag{25}$$

## APPENDIX II: NOMENCLATURE

$B_H$ = horizontal eddy thermal diffusivity, cm$^2$/sec
$B_v$ = vertical eddy thermal diffusivity, cm$^2$/sec
$C_0$ = phase velocity of surface gravity waves = $\sqrt{(gH)}$, cm/sec
$C_p$ = specific heat at constant pressure, cal/gm -°C
$f$ = Coriolis parameter, sec$^{-1}$
$g$ = gravitational acceleration, cm/sec$^2$
$h$ = depth relative to the mean water level, cm
$H$ = depth contour relative to the free surface = $h + \eta$, cm
$I$ = grid index in $x$-direction or $\alpha$-direction
$J$ = index in y-direction or $\beta$-direction
$K$ = grid index in $z$-direction or $\sigma$-direction
$K_H$ = horizontal kinematic eddy viscosity, cm$^2$/sec
$K_v$ = vertical kinematic eddy viscosity, cm$^2$/sec
$K_s$ = surface heat transfer coefficient, cal/cm$^2$-sec-°C
$n$ = time level
$p$ = pressure, dyn/cm$^2$
$T$ = temperature, °C
$T_e$ = equilibrium temperature, °C
$T_i$ = initial temperature, °C
$T_s$ = surface temperatue, °C
$t$ = time, sec
$u$ = velocity component in $x$-direction, cm/sec
$v$ = velocity component in y-direction, cm/sec
$w$ = velocity component in $z$-direction, cm/sec

$x$ = horizontal co-ordinate, cm
$y$ = horizontal co-ordinate, cm
$z$ = vertical position relative to the mean water level, cm
$Z$ = vertical position relative to the free surface = $z + \eta$, cm

*Greek symbols*

$\alpha$ = horizontal co-ordinate in stretched system = $x$, cm
$\beta$ = horizontal co-ordinate in stretched system = $y$, cm
$\sigma$ = vertical co-ordinate in stretched system, $Z/H$
$\Omega$ = transformed (or equivalent) vertical velocity, $sec^{-1}$
$\rho$ = density, $gm/cm^3$
$\eta$ = free surface elevation above mean water level, cm
$\tau_{xz}$ = surface shear stress in $x$-direction, $dyn/cm^2$
$\tau_{yz}$ = surface shear stress in $y$-direction, $dyn/cm^2$

*Subscripts and superscripts*

$H$ = horizontal quantity
$i$ = initial
interior = quantity at interior point one grid step from lateral boundary, for momentum equation
$n$ = one time level back
$n+1$ = current time level
$n-1$ = two time levels back
0 = quantity at inlet
$S$ = surface quantity
$V$ = vertical quantity
$W$ = lateral boundary
$W+1$ = quantity at interior point one grid step from later boundary, for energy equation
$xz$ = quantity in $x$-direction, normal to $z$-direction
$yz$ = quantity in $y$-direction, normal to $z$-direction
$\bar{(\ )}$ = arithmetic mean of quantity

## REFERENCES

1. S. S. Lee and S. Sengupta, 'Three-dimensional thermal pollution models', *Final Report NASA CR-144858* (1977).
2. J. J. Leendertse, R. C. Alexander and S. K. Liu, 'A three dimensional model for estuaries and coastal seas', *Principles of Computation Volume* 1, Rand Corporation, Dec. (1973).
3. A. F. Blumberg, 'Numerical tidal model of Cheasapeake Bay', *Hydraulics Div. ACSE* (1977).
4. A. F. Blumberg, 'Numerical model of estuarine circulation', *Hydraulics Div. ASCE* (1977).
5. R. O. Reid and B. R. Bodine, 'Numerical model for storm surges in Galveston Bay', *Proc. J Waterways and Harbors Div. ASCE*, 33-37 Feb. (1968).
6. H. B. Fischer, 'Mixing and dispersion in estuaries', *Annal. Rev. Fluid Mech.*, **8** (1976).
7. A. P. Verma and A. M. Dean, 'Numerical modelling of hydromechanics of bay systems', Department of Coastal and Oceanographic Engineering, University of Florida (1969).
8. S. Sengupta, S. S. Lee and R. Bland, 'Three-dimensional model development for thermal pollution studies', *Proc. EPA Conf. on Modelling*, Cincinnati (1976).
9. S. Sengupta, S. S. Lee and C. V. Carter, 'Three-dimensional time dependent simulations of hydrothermal behavior of Biscayne Bay', *Applied Mathematical Modelling*, **4**, February (1980).
10. J. J. Schneider, 'Tidal relations in the south Biscayne Bay', *U.S. Geological Survey* (1969).
11. A. F. Blumberg, 'The influences of density variations on estuarine tides and circulations', *Estuarine and Coastal Marine Science* (1978).

12. S. Sengupta, S. S. Lee and S. Miller, 'Three-dimensional free-surface model for transport processes in Biscayne Bay', *Computing Methods in Geophysical Mechanics, ASME*, AMD, **25** (1977).
13. S. Sengupta and W. Lick, 'A numerical model for wind-driven circulation and heat transfer in lakes and ponds', *FTAS/TR*–74–98 (1974).
14. N. A. Phillips, 'A coordinate system having some special advantages for numerical forecasting', *J. Meteorology*, **14,** (1957).
15. N. G. Freeman, A. M. Hale and M. B. Danard, 'A modified sigma equations approach to the numerical modelling of great lakes hydrodynamics', *J. Geophys. Research*, **77,** No. 6 (1972).
16. T. N. Veziroglu, S. S. Lee, H. W. Hiser, N. Weinberg and S. Sengupta, 'The application of remote sensing to detecting thermal pollution', *Mid-term Report NAS*–10–8740 (1975).
17. P. J. Roache, *Computational Fluid Dynamics*, Hermosa Publishers, 1972.
18. B. W. Wilson, 'Notes on surface wind stresses over water at low and high wind speeds', *J. Geophys. Research*, **65,** No. 10 (1960).
19. J. E. Edinger and J. C. Geyer, 'Heat exchange in the environment', *E.E.I. Publication, No.* 65–902, Edison Electric Institute (1971).
20. D. R. F. Harleman and K. D. Stolzenbach, 'Engineering and environmental aspects of heat disposal from power generation', Department of Civil Engineering, Massachusetts Institute of Technology, June (1975).
21. A. T. Ippen (ed.), *Estuary and Coastline Hydrodynamics*, McGraw-Hill, New York, 1966.